Microstrip Excitation of Magnetostatic Surface Waves: Theory and Experiment

ACHINTYA K. GANGULY AND DENIS C. WEBB, MEMBER, IEEE

Abstract—A model is developed for excitation of magnetostatic surface waves (MSSW) with microstrip transmission lines. Energy carried away in MSSW propagating perpendicular to the microstrip is related to electromagnetic (EM) energy propagating along the microstrip line by an equivalent radiation resistance. Supporting experimental results are in excellent agreement with predictions derived from this model.

I. INTRODUCTION

MAGNETOSTATIC surface waves (MSSW) are potentially important for carrying out signal processing directly at microwave frequencies because of their low propagation loss, ease of excitation, and possibility for electrically variable delay. Operation of MSSW delay lines has been demonstrated from 1 to 15 GHz [1], [2]; much higher frequency operation appears feasible. Thus MSSW devices are in a sense complementary to surface acoustic-wave (SAW) devices in that their useful frequency range begins at frequencies where problems of fabrication and loss begin to make SAW devices impractical.

A central problem in development of useful MSSW devices and in particular in designing suitable matching circuitry is the characterization of the excitation efficiency, or equivalently, the radiation resistance, in terms of geometrical and material parameters. Previous investigators have calculated dispersive characteristics [3], [4] and characteristic impedances [5] of composite dielectric–magnetic slab structures. However, the problem of surface-wave excitation has not been considered.

Microstrip excitation of MSSW has proven particularly convenient [1], [3]. Because coupling from electromagnetic (EM) waves to MSSW is very strong a single metallic strip rather than a meander line is sufficient. This is in contrast to SAW excitation where an interdigital transducer is necessary. In this paper we consider two different excitation geometries, shown in Fig. 1. Configuration *A* is somewhat easier to implement and enables several samples to be evaluated with a common microstrip line. Our experiments therefore concentrated on this geometry. Configuration *B* is useful for constructing totally planar configurations. As will be pointed out later in the text, the two geometries exhibit somewhat different excitation properties.

Manuscript received April 23, 1975; revised July 28, 1975.
The authors are with the Naval Research Laboratory, Washington, D.C. 20375.

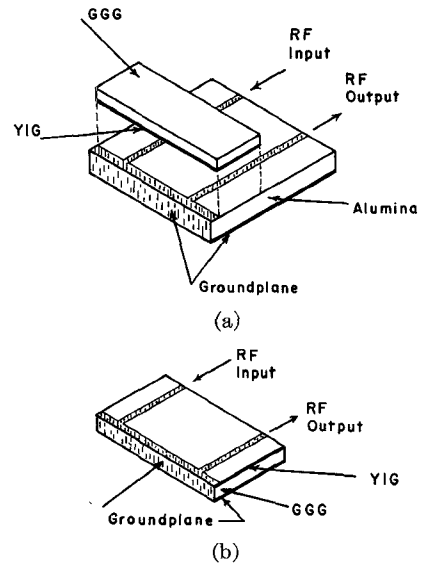

Fig. 1. Microstrip excitation of MSSW. (a) Using a standard alumina substrate (configuration *A*). (b) Using a GGG substrate (configuration *B*).

The approach used in this paper for calculating the radiation resistance is basically one of power conservation. In Section II the electric and magnetic fields associated with MSSW are obtained by solving Maxwell's equations with appropriate boundary conditions at the various interfaces. Magnetic anisotropy and magnetic relaxation are included. The current carried in the microstrip line is approximated as a surface current which is uniform within the microstrip and zero outside of it. This introduces an inhomogeneous boundary condition on the tangential component of the magnetic field at the interface containing the microstrip. The effects of reflection of MSSW at the edges of the microstrip are not considered. Results for the magnetostatic approximation are obtained from the solution of Maxwell's equations by assuming that the wavelength of MSSW are much shorter than that of EM waves at the same frequency. Since there is no significant difference in the values of radiation resistance calculated from the full Maxwell equations and the magnetostatic approximation, the magnetostatic approximation was employed in most of the numerical calculations. In Section III the complex Poynting theorem is used to determine the radiation impedance, $Z_m = R_m + iX_m$, of an infinitely long YIG-loaded microstrip transmission line. The input impedance Z_i of a shorted transmission line is, in general, a complex quantity involving the propa-

gation constant and characteristic impedance of the line as well as Z_m. When the total attenuation and phase shift through the shorted section are not large, a condition met in many cases of experimental interest, the real part of Z_i can be approximated by $R_m l/2$, where l is the length of the transmission line. Although we present results for only the real part of Z_i, a method for determining the imaginary part is also suggested. Finally, the experimental techniques employed in verifying the theory are discussed in Section IV; experimental results are summarized in Section V.

II. TE MODES

The system shown in Fig. 1(a) (configuration A) will be considered in detail. That shown in Fig. 1(b) (configuration B) can be analyzed by a straightforward extension of this case; hence, only pertinent results will be quoted. A cross-sectional view of the geometrical configuration is shown in Fig. 2. It consists of a three-layered semi-infinite slab. A magnetic layer having a tensor permeability, $\ddot{\mu}$, is sandwiched between two dielectric regions. The microstrip line for excitation of MSSW lies between the magnetic region (II) and a dielectric region (III). Note that this dielectric region corresponds to that of the alumina substrate [Fig. 1(a)]. Perfect conductors are assumed. The z axis is taken parallel to the internal magnetic bias field $\boldsymbol{H}_0$. $\boldsymbol{H}_0$ is the sum of an externally applied static magnetic field $\boldsymbol{H}_a$ and the anisotropy field $\boldsymbol{H}_A$.

Since the geometry is assumed uniform and infinite in the z direction, solutions to Maxwell's equations are of two types of modes, those derivable from E_z and those derivable from H_z. We will consider only transverse electric waves (components E_z, H_x, and H_y) propagating in the y direction. The constitutive equations to be used with Maxwell's equations are

$$\boldsymbol{B} = \mu_0 \ddot{\mu}_r \cdot \boldsymbol{H} \quad \text{and} \quad \boldsymbol{D} = \epsilon_0 \ddot{\epsilon}_r \cdot \boldsymbol{E} \tag{1}$$

where μ_0 and ϵ_0 are the vacuum permeability and dielectric constant, respectively. The general expression for the relative permeability, μ_r, in anisotropic media, including the effect of damping, has been given by Vittoria and Wilsey [6]. In both air (region I) and the dielectric layer (region III), μ_r is a unit matrix. It will be assumed that the dielectric properties are isotropic in the three regions I, II, and III, and the relative dielectric constants, ϵ_r, in these regions will be denoted by ϵ_1, ϵ_2, and ϵ_3, respectively.

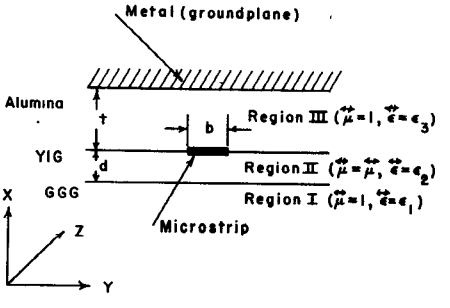

Fig. 2. Cross-sectional view of the excitation geometry [Fig. 1(a)]. The origin is taken at the interface between Regions II and III at the centerline of the microstrip. The internal magnetic bias field lies along the $+z$ direction.

The solutions for the TE modes of the system may be written as follows.

Region I: $-\infty < x < -d$

$$B_x = \mu_0 H_x = \mu_0 \int_{-\infty}^{+\infty} A_k \exp(\beta_1 \mid k \mid x) \cdot \exp[-i(ky - \omega\tau)]\, dk$$

$$H_y = -i \int_{-\infty}^{+\infty} s\beta_1 A_k \exp(\beta_1 \mid k \mid x) \cdot \exp[-i(ky - \omega\tau)]\, dk. \tag{2}$$

H_x and H_y are chosen so that they tend to zero at $x = -\infty$. Here $s = k/\mid k \mid$, the sign of k.

Region II: $-d < x < 0$

$$B_x = \mu_0 \int_{-\infty}^{+\infty} \left\{ \frac{\mu_{11}\mu_{22} - \mu_{12}^2}{\mu_{11}\beta_2 + \mu_{12}s} B_k \exp(\beta_2 \mid k \mid x) - \frac{\mu_{11}\mu_{22} - \mu_{12}^2}{\mu_{11}\beta_2 - \mu_{12}s} C_k \exp(-\beta_2 \mid k \mid x) \right\} \cdot \exp[-i(ky - \omega t)]\, dk$$

$$H_y = -i \int_{-\infty}^{+\infty} [sB_k \exp(\beta_2 \mid k \mid x) + sC_k \exp(-\beta_2 \mid k \mid x)] \cdot \exp[-i(ky - \omega\tau)]\, dk. \tag{3}$$

Region III: $0 < x < t$

$$B_x = \mu_0 \int_{-\infty}^{+\infty} [D_k \exp(\beta_3 \mid k \mid x) - E_k \exp(\beta_3 \mid k \mid x)] \cdot \exp[-i(ky - \omega\tau)]\, dk$$

$$H_y = -i \int_{-\infty}^{+\infty} s\beta_3 [D_k \exp(\beta_3 \mid k \mid x) + E_k \exp(-\beta_3 \mid k \mid x)] \cdot \exp[-i(ky - \omega\tau)]\, dk. \tag{4}$$

Expressions for E_z are obtained from that of B_x by multiplying the integrand with $\omega s/\mid k \mid$. In (2)–(4) β_1, β_2, and β_3 are given by

$$\beta_1 = [1 - (\omega/c_0 k)^2]^{1/2} \tag{5}$$

$$\beta_2 = (\mu_{22}/\mu_{11})^{1/2}[1 + (\epsilon_2^{1/2}\omega/c_0 k)^2(\mu_{12}^2 - \mu_{11}\mu_{22})/\mu_{11}]^{1/2} \tag{6}$$

$$\beta_3 = [1 - (\epsilon_3^{1/2}\omega/c_0 k)^2]^{1/2} \tag{7}$$

where $c_0 = 1/(\mu_0\epsilon_0)^{1/2}$ is the velocity of light in vacuum.

The coefficients A, B, C, D, and E are determined from the following boundary conditions: $B_x = 0$ at $x = t$ and is continuous at $x = 0$ and $-d$; H_y is continuous at $x = -d$ and discontinuous by j_0, the surface current density, at $x = 0$. We consider the microstrip to be of negligible thickness and incorporate it in the boundary conditions as a surface current. We take the following form for j_0:

$$j_0 = (I_0/b) \exp [i(\omega\tau)], \qquad |y| < b/2 \tag{8}$$

$$= 0, \qquad |y| > b/2 \tag{9}$$

where I_0 is the current in the microstrip of width b.

From (2)–(9), using the inverse Fourier transform, we get

$$A_k = -\frac{iI_0 s}{2\pi} \cdot \frac{\sin (bk/2)}{(bk/2)} \cdot \frac{(\alpha_1 + \alpha_2)(1/\beta_3) \tanh \beta_3 |k| t}{F(k,\omega)} \cdot \exp [-(\beta_2 - \beta_1)|k| d]$$

$$B_k = -\frac{iI_0 s}{2\pi} \cdot \frac{\sin (bk/2)}{(bk/2)} \cdot \frac{(\alpha_1\beta_1 + 1)(1/\beta_3) \tanh \beta_3 |k| t}{F(k,\omega)}$$

$$C_k = -\frac{iI_0 s}{2\pi} \cdot \frac{\sin (bk/2)}{(bk/2)} \cdot \frac{(\alpha_2\beta_1 - 1)(1/\beta_3) \tanh \beta_3 |k| t}{F(k,\omega)} \cdot \exp (-2\beta_2 |k| d)$$

$$E_k = \frac{iI_0 s}{2\pi} \cdot \frac{\sin (bk/2)}{(bk/2)} \cdot \frac{1}{\beta_3[1 + \exp (2\beta_3 |k| t)]} \cdot \frac{\alpha_2(\alpha_1\beta_1 + 1) - \alpha_1(\alpha_2\beta_1 - 1) \exp (-2\beta_2 |k| d)}{F(k,\omega)}$$

$$D_k = E_k \exp (-2\beta_3 |k| t) \tag{10}$$

where α_1 and α_2 are given by

$$\alpha_1 = \frac{\mu_{11}\mu_{22} - \mu_{12}^2}{\mu_{11}\beta_2 - \mu_{12} s} \quad \text{and} \quad \alpha_2 = \frac{\mu_{11}\mu_{22} - \mu_{12}^2}{\mu_{11}\beta_3 + \mu_{12} s}. \tag{11}$$

The function $F(k,\omega)$ in (10) is defined by

$$F(k,\omega) = (\alpha_1\beta_1 + 1)[\alpha_2 + (1/\beta_3) \tanh \beta_3 |k| t] - (\alpha_2\beta_1 - 1)[\alpha_1 - (1/\beta_3) \tanh \beta_3 |k| t] \cdot \exp (-2\beta_2 |k| d). \tag{12}$$

The surface-wave propagation takes place at wave vector $|k| = k_{0s}$ given by [7]

$$F(k_{0s},\omega) = 0. \tag{13}$$

The ω versus k_{0s} curves may have two branches [5], [8]—the lower branch falling within the frequency limits $0 < \omega < \omega_m$, while for the upper branch $\omega > \omega_m$.

$$\omega_m = \gamma(H_0 + 4\pi M_0) \tag{14}$$

where γ is the gyromagnetic ratio and $4\pi M_0$ is the saturation magnetization. For YIG, $4\pi M_0 = 1750$ Oe at room temperature and $\gamma/2\pi = 2.8$ MHz/Oe. The lower branch corresponds to MSSW while the upper branch corresponds to "dynamic" waves [8]. Since we are interested only in MSSW excitation, the upper branch will be ignored although the theory is valid for the entire frequency spectrum. For a given frequency ω, k_{0s} will be different for $s = \pm 1$. In the following we will suppress the subscript s on k_0 for notational convenience.

The components of the electric and magnetic fields can be obtained by substituting (2)–(4) in Maxwell's equations. We thus obtain the following equations:

1) $-\infty < x < -d$

$$B_x = -i\mu_0 \int_{-\infty}^{+\infty} G(k,\omega)(\alpha_1 s + \alpha_2 s) \exp [\beta_1 |k| (x + d)] \cdot \exp (-iky)\, dk/F(k,\omega)$$

$$H_y = -\int_{-\infty}^{+\infty} \beta_1 G(k,\omega)(\alpha_1 + \alpha_2) \exp [\beta_1 |k| (x + d)] \cdot \exp (-iky)\, dk/F(k,\omega) \tag{15}$$

2) $-d < x < 0$

$$B_x = -i\mu_0 \int_{-\infty}^{+\infty} G(k,\omega)\{\alpha_2 s(\alpha_1\beta_1 + 1) \exp [\beta_2 |k| (x + d)] - \alpha_1 s(\alpha_2\beta_1 - 1) \exp [-\beta_2 |k| (x + d)]\} \cdot \exp (-iky)\, dk/F(k,\omega)$$

$$H_y = -\int_{-\infty}^{+\infty} G(k,\omega)\{(\alpha_1\beta_1 + 1) \exp [\beta_2 |k| (x + d)] + (\alpha_2\beta_1 - 1) \exp [-\beta_2 |k| (x + d)]\} \cdot \exp (-iky)\, dk/F(k,\omega) \tag{16}$$

3) $0 < x < t$

$$B_x = -i\mu_0 \int_{-\infty}^{+\infty} G(k,\omega)\{\alpha_2 s(\alpha_1\beta_1 + 1) \exp (\beta_2 |k| d) - \alpha_1 s(\alpha_2\beta_1 - 1) \exp (-\beta_2 |k| d)\} \cdot \frac{\sinh \beta_3 |k| (t - x)}{\sinh \beta_3 |k| t} \exp (-iky)\, dk/F(k,\omega)$$

$$H_y = -\int_{-\infty}^{+\infty} G(k,\omega)\{(\alpha_1\beta_1 + 1) \exp (\beta_2 |k| d) + (\alpha_2\beta_1 - 1) \exp (-\beta_2 |k| d)\} \frac{\cosh \beta_3 |k| (t - x)}{\cosh \beta_3 |k| t} \cdot \exp (-iky)\, dk/F(k,\omega) + H_{y3}^{(0)} \tag{17}$$

where

$$H_{y3}^{(0)} = \frac{I_0 \exp (+i\omega\tau)}{2\pi} \int_{-\infty}^{+\infty} \frac{\sin (bk/2)}{(bk/2)} \cdot \frac{\cosh \beta_3 |k| (t - x)}{\cosh \beta_3 |k| t} \cdot \exp (-iky)\, dk. \tag{18}$$

In (15)–(17) $G(k,\omega)$ is given by

$$G(k,\omega) = \frac{I_0 \exp (i\omega\tau)}{2\pi} \cdot \frac{\sin (bk/2)}{(bk/2)} \cdot \frac{\exp (-\beta_2 |k| d) \tanh \beta_3 |k| t}{\beta_3}. \tag{19}$$

The term $H_{y3}^{(0)}$ in (17) takes into account the discontinuity in H_y at $x = 0$. Setting $x = 0$ in (18), it is easy to see that $H_{y3}^{(0)} = (I_0/b) \exp (+i\omega\tau)$ for $|y| \leq b/2$ and zero otherwise. All other terms in the expressions for B_x, H_y, and E_z are continuous at the interfaces at $x = 0$ and

$-d$. These terms have the general form

$$\int_{-\infty}^{+\infty} \frac{\sin (bk/2)}{(bk/2)} \frac{Q(k,\omega)}{F(k,\omega)}\, dk.$$

It can be shown that all derivatives of $F(k,\omega)$ exist at $k = k_0$ and the first derivative is nonzero. Therefore, $F(k,\omega)$ has a simple zero at $k = k_0$ and we can write

$$F(k,\omega) = (k - k_0) \sum_{n=1}^{\infty} F^{(n)}(k_0,\omega) \frac{(k - k_0)^{n-1}}{n!} \quad (20)$$

where $F^{(n)}(k_0,\omega)$ is the nth derivative of F with respect to k evaluated at $k = k_0$. By differentiating (12) we have

$$F^{(1)}(k_0,\omega) = 2sd\beta_2 A_{k0}(\alpha_1\beta_1 + 1)(\alpha_2 + (1/\beta_3)\tanh \beta_3 k_0 t) \quad (21)$$

where

$$A_{k0} = 1 + \frac{t}{2\beta_2 d} \cdot \frac{(\alpha_1 + \alpha_2)(1 - \tanh^2 \beta_3 k_0 t)}{(\alpha_1\beta_3 - \tanh \beta_3 k_0 t)(\alpha_2\beta_3 + \tanh \beta_3 k_0 t)\beta_3^2}$$

$$- \frac{(\omega/c_0 k)^2}{2\beta_2 k_0 d}\left[\frac{(\alpha_1 + \alpha_2)}{(\alpha_1\beta_1 + 1)(\alpha_2\beta_1 - 1)\beta_1}\right.$$

$$+ \frac{k_0 d(\mu_{12}^2 - \mu_{11}\mu_{22})\epsilon_2}{\mu_{11}\beta_2}$$

$$+ \frac{\epsilon_3(\alpha_1 + \alpha_2)\{\tanh \beta_3 k_0 t - \beta_3 k_0 t(1 - \tanh^2 \beta_3 k_0 t)\}}{\beta_3(\alpha_1\beta_3 - \tanh \beta_3 k_0 t)(\alpha_2\beta_3 + \tanh \beta_3 k_0 t)}$$

$$- \frac{\epsilon_2(\beta_3 + \beta_1 \tanh \beta_3 k_0 t)}{\beta_2}$$

$$\cdot \left\{\frac{\alpha_1^2}{(\alpha_1\beta_1 + 1)(\alpha_1\beta_3 - \tanh \beta_3 k_0 t)}\right.$$

$$\left.\left. + \frac{\alpha_2^2}{(\alpha_2\beta_1 - 1)(\alpha_2\beta_3 + \tanh \beta_3 k_0 t)}\right\}\right]. \quad (22)$$

Since $F(k,\omega)$ has simple pole at $k = k_0$, we may evaluate the integrals by the method of contour integration in complex k plane. The contour will consist of the real k axis and an infinite semicircle on the upper half-plane so that outgoing waves in the $+y$ and $-y$ directions are obtained. We ignore the effects of reflection at the edges of the microstrip. Sin $(bk/2)$ is not well behaved on the upper half of the complex k plane. In order to avoid that difficulty we break up the integrands into two terms by writing

$$\frac{1}{F(k,\omega)} = \frac{1 - F(k,\omega)/F(\infty,\omega)}{F(k,\omega)} + \frac{1}{F(\infty,\omega)} \quad (23)$$

where

$$F(\infty,\omega) = (\alpha_1\beta_1 + 1)(\alpha_2/\beta_3 + 1)/\beta_3. \quad (24)$$

Each of the integrals in (15)–(17) will thus separate into two parts. We consider first the part arising from the first term in (23). These contributions to the field components will be denoted by a superscript (1). This part may now be evaluated by contour integration since the integrands are now well behaved, except for the pole at $k = k_0$. By applying the method of residues we obtain the equations for all the field components. We write down explicitly only those components which we will later need in the calculation of radiation resistance.

Region III: $0 < x < t$

$$H_x^{(1)} = \frac{I_0 R_{k0}}{2\beta_2 d} \cdot \frac{\sin (bk_0/2)}{(bk_0/2)} \cdot \frac{\exp(-\beta_3 k_0 t)}{\beta_3[1 + \exp(-2\beta_3 k_0 t)]}$$

$$\cdot \left[\frac{\exp(\beta_2 k_0 d)}{\alpha_2\beta_1 - 1} + \frac{\exp(-\beta_2 k_0 d)}{\alpha_1\beta_1 + 1}\right][\exp[\beta_3 k_0(x - t)]$$

$$- \exp[\beta_3 k_0(x - t)]] \exp[-i(k_0 ys - \omega\tau)] \quad (25)$$

where

$$R_{k0} = (\alpha_2\beta_1 - 1)\exp(-\beta_2 k_0 d)$$

$$\cdot \tanh \beta_3 k_0 t/(\alpha_2\beta_3 + \tanh \beta_3 k_0 t) A_{k0}. \quad (26)$$

Region II: $-d < x < 0$

$$H_x^{(1)} = \frac{I_0 R_{k0}}{2d} \cdot \frac{\sin (bk_0/2)}{(bk_0/2)}\left[\frac{\mu_{22}/\beta_2 + \mu_{12}s}{\mu_{11}\beta_2 + \mu_{12}s} \frac{\exp[\beta_2 k_0(x + d)]}{\alpha_2\beta_1 - 1}\right.$$

$$\left. - \frac{\mu_{22}/\beta_2 - \mu_{12}s}{\mu_{11}\beta_2 - \mu_{12}s} \frac{\exp[-\beta_2 k_0(x + d)]}{\alpha_1\beta_1 + 1}\right]$$

$$\cdot \exp[-i(k_0 ys - \omega\tau)]$$

$$H_y^{(1)} = \frac{-iI_0 sR_{k0}}{2\beta_2 d} \cdot \frac{\sin (bk_0/2)}{(bk_0/2)}\left[\frac{\exp[\beta_2 k_0(x + d)]}{\alpha_2\beta_1 - 1}\right.$$

$$\left. - \frac{\exp[-\beta_2 k_0(x + d)]}{\alpha_1\beta_1 + 1}\right] \exp[-i(k_0 ys - \omega\tau)]. \quad (27)$$

Region I: $-\infty < x < -d$

$$H_x^{(1)} = \frac{I_0 R_{k0}}{2\beta_2 d} \cdot \frac{\sin (bk_0/2)}{(bk_0/2)} \cdot \frac{\alpha_1 + \alpha_2}{(\alpha_1\beta_1 + 1)(\alpha_2\beta_1 - 1)}$$

$$\cdot \exp[\beta_1 k_0(x + d)] \exp[-i(k_0 ys - \omega\tau)]. \quad (28)$$

In all the regions the electric field is given by $E_z^{(1)} = (\omega s/k_0)B_x^{(1)}$. $H_x^{(1)}$, $H_y^{(1)}$, and $E_z^{(1)}$ represent the respective components of the magnetic and electric fields associated with the surface spin-wave propagation. Their amplitudes have sin ξ/ξ variation with the width of the microstrip.

The magnetostatic approximation holds when $k_0 \gg \epsilon^{1/2}\omega/c_0$, c_0 being the velocity of light in vacuum. If we neglect terms of order $(\epsilon^{1/2}\omega/c_0 k_0)$ and higher, the following approximate forms for β_1, β_2, and β_3 are obtained from (5)–(7):

$$\beta_1 = 1 = \beta_3 \quad (29)$$

$$\beta_2 = (\mu_{22}/\mu_{11})^{1/2} \equiv \beta. \quad (30)$$

From (11), (22), (26), (29), and (30)

$$\alpha_1 = \mu_{11}\beta + \mu_{12}s \quad \text{and} \quad \alpha_2 = \mu_{11}\beta - \mu_{12}s \tag{31}$$

$$\frac{\mu_{22}/\beta_2 + \mu_{12}s}{\mu_{11}\beta_2 + \mu_{12}s} = \frac{\mu_{22}/\beta_2 - \mu_{12}s}{\mu_{11}\beta_2 - \mu_{12}s} = 1 \tag{32}$$

$$A_{k0} = 1 + \mu_{11}(t/d)(1 - \tanh^2 k_0 t) \cdot [\mu_{11}^2\beta^2 - (\mu_{12}s - \tanh k_0 t)^2]^{-1} \tag{33}$$

$$R_{k0} = (\mu_{11}\beta - \mu_{12}s - 1)\exp(-\beta k_0 d)\tanh k_0 t / A_{k0}(\mu_{11}\beta - \mu_{12}s + \tanh k_0 t). \tag{34}$$

The expressions for $H_x^{(1)}$, $H_y^{(1)}$, and $E_z^{(1)}$ under magnetostatic approximation can easily be written down by substituting (29)–(34) in (25)–(28).

The contributions to B_x, H_y, and E_z from the second term in (23) will be denoted by $B_x^{(0)}$, $H_y^{(0)}$, and $E_z^{(0)}$, respectively. In region III ($0 < x < t$) the term $H_{y3}^{(0)}$ of (17) will be included in $H_y^{(0)}$. $B_x^{(0)}$, $H_y^{(0)}$, $E_z^{(0)}$ represent the components of fields due to the current in the microstrip line when there is no coupling with the spin system. In general, numerical procedures are necessary to evaluate these quantities. However, simple expressions for $B_x^{(0)}$ and $H_y^{(0)}$ under magnetostatic approximation can be obtained in all the regions for the cases where $t \to \infty$. For example, in Region I ($-\infty < x < d$)

$$B_x^{(0)} = -2\mu_0\mu_{11}\beta A_{k0}\ln\frac{\{(\beta-1)d + |x|\}^2 + (y + b/2)^2}{\{(\beta-1)d + |x|\} + (y - b/2)^2}$$

$$H_y^{(0)} = -2\mu_{11}\beta A_{k0}\arctan\frac{b\{(\beta-1)d + |x|\}}{\{(\beta-1)d + |x|\}^2 + y^2 - b^2/4}. \tag{35}$$

$$\frac{1}{2}\int_S (\boldsymbol{E} \times \boldsymbol{H}^*)\cdot d\boldsymbol{S} = 0 \tag{36}$$

where S is the closed surface bounded by the yz planes at $x = t$ and $-\infty$, the xz planes at $y = +y_0$, and the xy planes at $z = 0$, Δz. For the MSSW modes considered here, $(E \times H^*)_z = 0$ and $(E \times H^*)_x = 0$ at $x = t$ and $x = \infty$. Thus the power lost per unit length W_L by the EM wave propagating along the strip in passing through the enclosed volume is given by

$$W_L = \text{Re}\,(s/2)\int_{-\infty}^{t} E_z^{(1)}H_x^{*(1)}\,dx = \text{Re}\,(P_+ + P_-) \tag{37}$$

where P_+ and P_- denote the surface integrals for a unit length over the two xz planes at $y = \pm y_0$ with normals pointing in the $+y$ and $-y$ directions, respectively. $s = \pm 1$ denotes the $+y$ and $-y$ MSSW propagation directions, respectively. Since $E_z^{(1)} = \omega s B_x^{(1)}/k_0$, we have from (36) and (37)

$$P_\pm = \frac{\mu_0\omega}{2}\left[\int_{-\infty}^{-d} |H_{xI}^{(1)}|^2\,dx + \int_{-d}^{0}\{\mu_{11}|H_{xII}^{(1)}|^2 - i\mu_{12}H_{xII}^{(1)*}H_{yII}^{(1)}\}\,dx + \int_0^t |H_{xIII}^{(1)}|^2\,dx\right]. \tag{38}$$

On substitution of $H_x^{(1)}$ and $H_y^{(1)}$ from (25)–(28) in (38), we get

$$P_\pm = \tfrac{1}{2}A_\pm |I_0|^2 \tag{39}$$

where

$$A_\pm = \frac{\mu_0\omega}{4|\beta_2|^2}|R_{k0}|^2\frac{1}{(k_0)d}\left|\frac{\sin(bk_0/2)}{(bk_0/2)}\right|^2\left[\left|\frac{\alpha_1+\alpha_2}{(\alpha_1\beta_1+1)(\alpha_2\beta_1-1)}\right|^2\frac{1}{2(\beta_3k_0)_R d} + \left|\frac{\exp(\beta_2k_0d)}{\alpha_2\beta_1-1} + \frac{\exp(-\beta_2k_0d)}{\alpha_1\beta_1+1}\right|^2 \cdot \frac{1-\exp[-4(\beta_3k_0)_R t] - 2(\beta_3k_0)_R\exp[-2(\beta_3k_0)_R t]\sin\{2(\beta_3k_0)_I t\}/(\beta_3k_0)_I}{2|\beta_3|^2|1+\exp(-2\beta_3k_0t)|^2(\beta_3k_0)_R d} + \frac{\alpha_2}{|\alpha_2\beta_1-1|^2}\left(\frac{\mu_{22}+\mu_{12}\beta_2 s}{\mu_{11}\beta_2+\mu_{12}s}\right)^* \cdot \frac{\exp[2(\beta_2k_0)_R d]-1}{2(\beta_2k_0)_R d} + \frac{\alpha_1}{|\alpha_1\beta_1+1|^2}\left(\frac{\mu_{22}-\mu_{12}\beta_2 s}{\mu_{11}\beta_2-\mu_{12}s}\right)^* \frac{1-\exp[-2(\beta_2k_0)_R d]}{2(\beta_2k_0)_R d} - \frac{\sin(\beta_2k_0)_I d}{(\beta_2k_0)_I d} \cdot \left\{\frac{\mu_{22}^* - \mu_{12}^*\beta_2^* s}{\mu_{11}^*\beta_2^* - \mu_{12}^* s}\cdot\frac{\alpha_2\exp[i(\beta_2k_0)_I d]}{(\alpha_2\beta_1-1)(\alpha_1^*\beta_1^*+1)} + \frac{\mu_{22}^* + \mu_{12}^*\beta_2^* s}{\mu_{11}^*\beta_2^* + \mu_{12}^* s}\cdot\frac{\alpha_1\exp[-i(\beta_2k_0)_I d]}{(\alpha_2^*\beta_1^*-1)(\alpha_1\beta_1+1)}\right\}\right]. \tag{40}$$

The fields in the other two regions have the same general functional dependence. $H_x^{(0)}$ and $H_y^{(0)}$ are fields associated with modes not propagating in the y direction which approach zero for $y \gg b$. Thus they do not contribute to the radiation impedance but rather give a small complex contribution to the characteristic impedance of the microstrip line.

III. RADIATION IMPEDANCE

The average power carried away by magnetostatic surface waves can be related to the power lost from the electromagnetic wave through the complex Poynting theorem

The symbols $(\cdots)_R$ and $(\cdots)_I$ in (40) denote, respectively, the real and imaginary parts of the quantity inside the parenthesis. k_0 is obtained by solving (13). α_1 and α_2 are given in (11). k_0, α_1, and α_2 depend on the value of s.

P_+ and P_- in (39) can be interpreted as the power radiated per unit length by the waves traveling in the $+y$ and $-y$ directions, respectively. Since we have assumed that the medium is infinite in the y directions, there are no reflected waves. Thus the total radiated power per unit length is the real part of P_T given by

$$P_T = P_+ + P_- = \tfrac{1}{2}(A_+ + A_-)|I_0|^2 \triangleq \tfrac{1}{2}Z_m|I_0|^2 \tag{41}$$

where $Z_m = R_m + iX_m$ is the equivalent radiation impedance for an infinitely long microstrip line. Z_m will be real when the ferromagnetic linewidth $\Delta H = 0$. In the frequency range [3] $\gamma(H_0 + 2\pi M_0) < \omega < \gamma(H_0 + 4\pi M_0)$ the wave propagation is not allowed in the $-y$ direction. Z_m is then equal to A_+.

To this point only configuration A has been considered. Analysis of configuration B proceeds exactly as before, with the discontinuity in H_y occurring at $x = -d$. For configuration B we find that the fields $H_x^{(1)}$ and $H_y^{(1)}$ can be derived from the expressions given in (25)–(28) by simply omitting the factor

$$\frac{(\alpha_2\beta_1 - 1)\cdot\exp(-\beta_2 k_0 d)}{(\alpha_2\beta_3 + \tanh \beta_3 k_0 t)} \tanh \beta_3 k_0 t.$$

Furthermore, $A_\pm$ is now given by (40) with $R_{k0} = 1/A_{k0}$.

If the damping of the surface waves is neglected and the magnetostatic approximation made, then we have from (29)–(31) and (40)

$$A_\pm = \mu_0\omega R_{k0}^2 \left|\frac{\sin(bk_0/2)}{(bk_0/2)}\right|^2 [2\beta k_0 d\{(\mu_{12}s + 1)^2 - \mu_{11}^2\beta^2\}]^{-2}$$
$$\cdot \left[2\frac{1 - 4k_0 t \exp(-2k_0 t) - \exp(-4k_0 t)}{[1 + \exp(-2k_0 t)]^2}\right.$$
$$\cdot \{(\mu_{12}s + 1)\sinh(\beta k_0 d) + \mu_{11}\beta\cosh(\beta k_0 d)\}^2$$
$$+ (\mu_{12}s + 2\mu_{11}\beta^2 k_0 d)\{(\mu_{12}s + 1)^2 - \mu_{11}^2\beta^2\}$$
$$- \{\mu_{12}s[(\mu_{12}s + 1)^2 - \mu_{11}^2\beta^2] - 2\mu_{11}^2\beta^2\}\cosh(2\beta k_0 d)$$
$$\left. - \mu_{11}\beta(\mu_{12}^2 - 1 - \mu_{11}^2\beta^2)\sinh(2\beta k_0 d)\right]. \quad (42)$$

μ_{11}, μ_{22}, and μ_{12} are obtained from [6, eq. (8)] by setting the damping parameter $\lambda = 0$. R_{k0} is given by (34).

A particularly simple form for the radiation resistance R_m can be obtained when $t \to \infty$. By using the dispersion relation for MSSW, we obtain, after some manipulation from (42),

$$A_\pm = \frac{\mu_0\omega}{2}\left(\frac{\sin(bk_0/2)}{(bk_0/2)}\right)^2 \frac{\mu_{11}}{k_0 d[(\mu_{12} \mp 1)^2 - \mu_{11}\mu_{22}]} \quad (43)$$

where

$$k_0 d = \left(\frac{\mu_{11}}{\mu_{22}}\right)^{1/2} \ln\left[1 + \frac{4(\mu_{11}\mu_{22})^{1/2}}{\mu_{12}^2 - [(\mu_{11}\mu_{22})^{1/2} + 1]^2}\right]. \quad (44)$$

k_0 is independent of the direction of propagation when $t \to \infty$. Equation (43) holds for configuration A. For configuration B the roles of A_+ and A_- are interchanged. Therefore the radiation resistance $R_m = \text{Re}(A_+ + A_-)$ is the same in both configurations and given by

$$R_m = \mu_0\omega\left[\frac{\sin(bk_0/2)}{(bk_0/2)}\right]^2$$
$$\cdot \frac{\mu_{11}(\mu_{12}^2 + 1 - \mu_{11}\mu_{22})}{k_0 d[(\mu_{12} + 1)^2 - \mu_{11}\mu_{22}][(\mu_{12} - 1)^2 - \mu_{11}\mu_{22}]}. \quad (45)$$

In Fig. 3 the radiation resistance (R_m) is plotted as a function of frequency. The curves marked (a) and (b) denote, respectively, R_m in configurations A and B. The solid curves are obtained from Maxwell's equations while the magnetostatic approximation is used for the dashed curves. As seen from the figure, there is no significant difference in the results obtained by the two methods. In all subsequent calculations magnetostatic approximation will be used to save computation time.

The ratio of Re (A_+) to Re (A_-) gives the ratio of power delivered to the + and − directions, respectively. This is illustrated in Fig. 4 for the two excitation configurations. Unlike SAW excitation where $P_-/P_+ = 1$, $P_+ \neq P_-$ in general for MSSW and essentially unidirectional excitation is possible. Furthermore, the roles of the + and − waves become interchanged for the two configurations in the higher portion of the frequency range (high k). This is because the two oppositely propagating waves have amplitude maxima on opposite sides of the YIG film surface and the microstrip most strongly excites

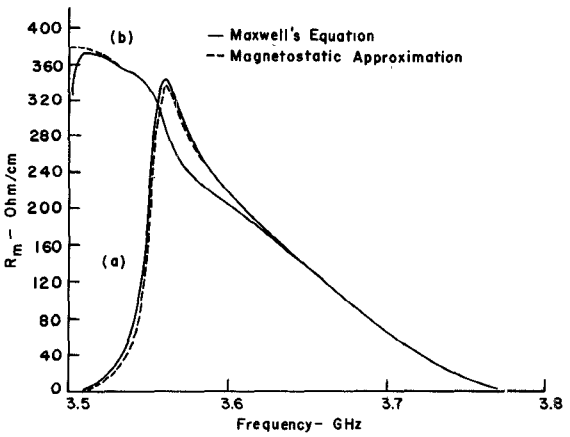

Fig. 3. Radiation resistance R_m versus frequency obtained from Maxwell's equations (solid curves) and the magnetostatic approximation (dashed curves). Curves marked (a) and (b) refer, respectively, to the configurations of Fig. 1(a) and (b). Parameters used are: $t = 254$ μm; $b = 178$ μm; $H_0 = 650$ Oe; $\epsilon_2 = \epsilon_3 = 10$; $d = 6.25$ μm.

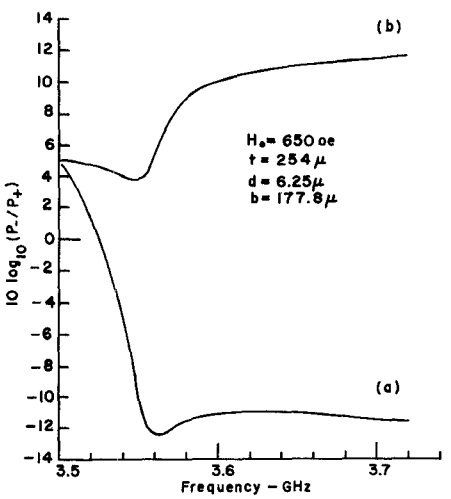

Fig. 4. Relative power carried by MSSW propagating in the $+y$ and $-y$ directions. Curves marked (a) and (b) refer, respectively, to the configurations of Fig. 1(a) and (b).

the wave having the largest amplitude at the surface where the strip is located.

The calculated radiation resistance will now be related to experimentally measurable parameters. We assume that the voltage and current of the EM wave propagating along the microstrip line are of the form $\exp[-\alpha_0 z - i(\beta_0 z - \omega\tau)]$, where α_0, the attenuation constant, arises solely from excitation of the MSSW modes. Furthermore, the voltage and current are related by a characteristic impedance Z_0. The average power carried by the transmission line is

$$P = \tfrac{1}{2} Z_0 \mid I_m \mid^2. \tag{46}$$

Also

$$W_L = \frac{\partial P}{\partial z} = 2\alpha_0 P. \tag{47}$$

From (37), (41), (46), (47), and equating I_0 to I_m we obtain

$$Z_m = 2\alpha_0 Z_0. \tag{48}$$

For optimum MSSW excitation the YIG line should be terminated in a short circuit. Experiment and theory will therefore be related for this configuration (Fig. 5). The characteristic impedance and propagation constant are in general different for the YIG-loaded and unloaded microstrip sections. These quantities were recently determined by Wu and Rosenbaum for the YIG microstrip structure [5]. At the junction of the two lines, the impedance Z_i, seen looking toward the short, is

$$Z_i = R_i + iX_i = Z_0 \tanh(\alpha_0 + i\beta_0)l. \tag{49}$$

From (48) and (49)

$$Z_m = 2\alpha_0 Z_i / \tanh(\alpha_0 + i\beta_0)l. \tag{50}$$

Experiments [5] have shown that the imaginary part of Z_0 is smaller than the real part by at least an order of magnitude. In this approximation, it can be shown that

$$R_m = \frac{2R_i\alpha_0}{\tanh \alpha_0 l} \frac{1 + \tanh^2 \alpha_0 l \tan^2 \beta_0 l}{1 + \tan^2 \beta_0 l} \tag{51}$$

$$X_m = \frac{\mathrm{Im}(Z_0)}{\mathrm{Re}(Z_0)} \cdot R_m. \tag{52}$$

When $\alpha_0 l \ll 1$ and $\beta_0 l \ll 1$, (51) reduces to

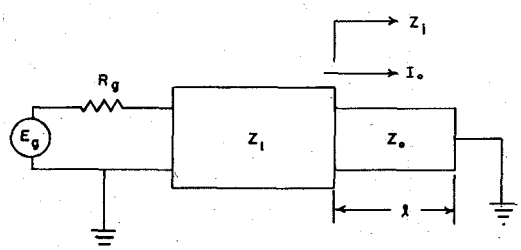

Fig. 5. Excitation of MSSW by a shorted transmission line. Subscript 1 denotes the unloaded section; subscript 0 denotes the YIG-loaded section.

$$R_m = 2\frac{R_i}{l}. \tag{53}$$

Reference [5] and experiments described in the following sections verify that this relationship is valid over a considerable range of experimental conditions of interest.

We can consider the transmission line Z_1 to be terminated in an impedance $Z_i = R_i + jX_i$. The ratio of the power P_m which is dissipated in R_i, i.e., converted to MSSW, to that delivered by the generator P_I is given by

$$\frac{P_m}{P_I} = \frac{4Z_1 R_i}{(R_i + Z_1)^2 + X_i^2}. \tag{54}$$

With $\alpha_0 l, \beta_0 l \ll 1$, this equation reduces to

$$\frac{P_m}{P_I} \approx \frac{2Z_1 R_m l}{(Z_1 + R_m l/2)^2}. \tag{55}$$

Since essentially unidirectional excitation is possible and $R_m l/2$ can approach $Z_1 (Z_0 > Z_1$ from [5]), nearly total conversion from EM to MSSW energy is possible. Moreover, since (49) and (54) are general expressions, by using Z_0 and β_0 from [5] and α_0, determined here, both the real and imaginary parts of Z_i as well as the loss in conversion from EM to MSSW energy can be determined even when $\alpha_0 l, \beta_0 l \gtrsim 1$.

IV. EXPERIMENT

Both of the previously mentioned excitation schemes were investigated experimentally. A picture of the alumina substrate geometry used is shown in Fig. 6. Slices approximately 2 mm wide were cut from 3/4-in-diam GGG wafers on which YIG films ranging from 1.7 to 6.25 μm had been grown. (Dimensions of the individual samples evaluated are given in Fig. 7.) The samples were mounted on the microstrip line in the manner shown in Fig. 1(a). The microstrip circuit consisted of 0.18-mm-wide strips on a 0.25-mm-thick substrate. For these dimensions the characteristic impedance Z_i of the line is 60 Ω, and the ratio of free space to guide wavelengths, λ_0/λ, is 2.6 [9]. The

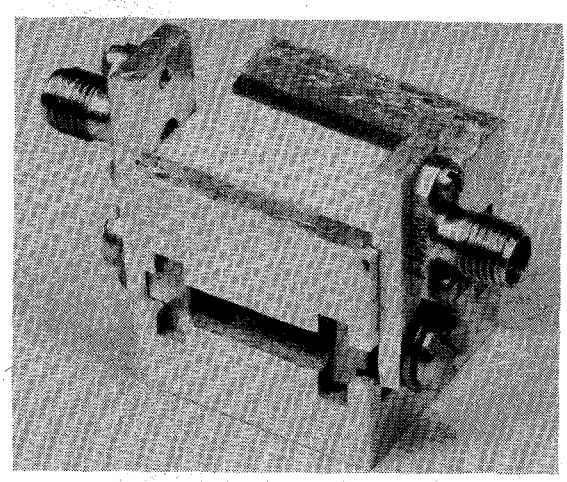

Fig. 6. Experimental alumina microstrip geometry.

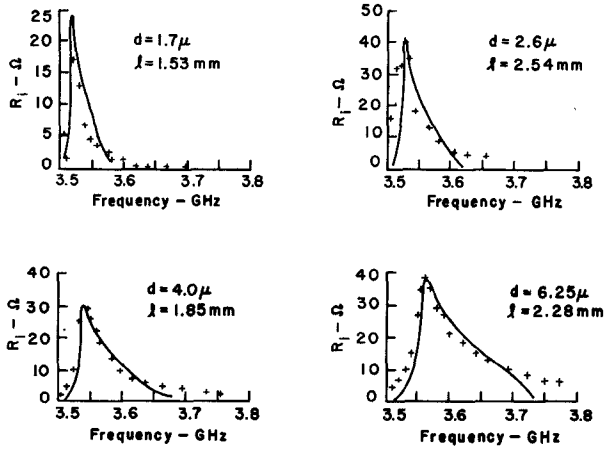

Fig. 7. Measured and computed values of the input resistance R for configuration A [Fig. 1(a)] for four different thickness YIG samples at $H_0 = 650$ Oe; $b = 177.8$ μm; and $t = 254$ μm (+, measured).

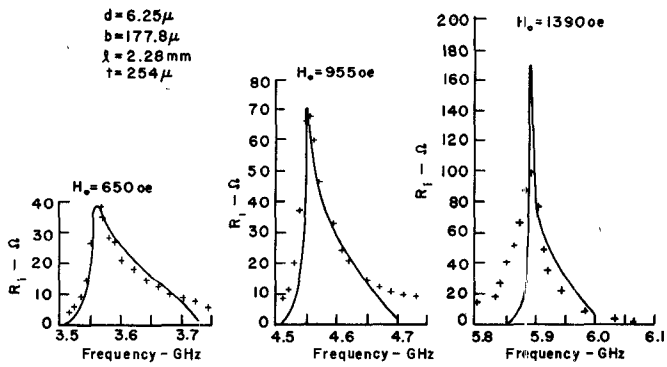

Fig. 8. Measured and computed values of the input resistance R_i for configuration A [Fig. 1(a)] (+, measured).

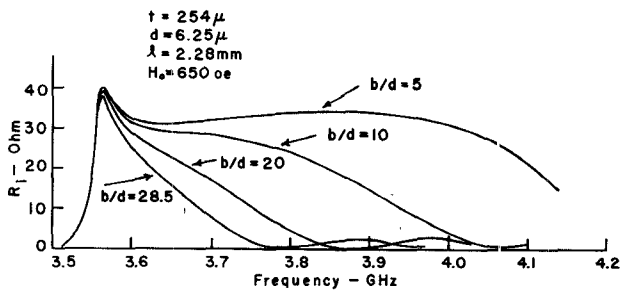

Fig. 9. R_i versus frequency with the ratio of microstrip width to film thickness b/d as a parameter.

latter number was verified by a time-domain reflectometer measurement. The required magnetic bias field in the plane of the film perpendicular to the long axis of the sample was provided with an electromagnet. The right-angle bend in the microstrip circuit minimized the magnet gap required.

A HP model 8545 automatic network analyzer was used to make the impedance measurements. Each individual series of measurements spanned a 400-MHz band of frequencies in 5-MHz steps. The magnetic bias field was adjusted to center the bands at one of three frequencies—3.5, 4.5, or 6.0 GHz. In order to compare the experimental and theoretical results, the measured input impedance to the microstrip circuit was translated along the microstrip transmission line to the front edge of the YIG/GGG sample using the values of Z_1 and λ/λ_0 cited in the previous paragraph.

Ohmic losses in the microstrip line were accounted for by taking the difference $R_i(H \neq 0) - R_i(H = 0)$. Essentially the same procedure was employed in investigating the configuration shown in Fig. 1(b). The microwave signal was first launched on a 50 Ω (0.025-in strip on a 0.025-in alumina substrate) microstrip line. It was then coupled to a 0.001-in-wide Cr–Au strip plated on the YIG/GGG sample by means of thermal-compression-bonded gold wire, 0.001-in in diameter. No matching sections were employed. A single YIG film sample was evaluated using this configuration. It was 6.2 μm thick and 0.5 cm wide.

V. RESULTS

Fig. 7 shows the theoretical and measured input resistance R_i of four different thickness YIG samples as a function of frequency at a constant magnetic bias field of 955 Oe. Fig. 8 shows the dependence of R_i upon bias field for a constant film thickness. All results are for the configuration A excitation geometry. In determining R_i (theoretical) the damping parameter, λ, is taken to be zero and the approximation $R_i = R_m l/2$ [(53)] is used. Note that the midband conversion loss, as determined by (55) [$= 10 \log (P_m/P_I)$] with $Z_1 \sim 50$ Ω is less than 1 dB for the range of experimental parameters shown.

Agreement between theory and experiment is, in general, excellent. The following trends can be observed for the range of experimental parameters considered: 1) at a fixed bias field and given microstrip geometry, the excitation bandwidth B_m increases approximately proportional to the YIG film thickness d. The maximum value of R_m increases only slightly with increasing d. Most of the variation in the maximum value of $R_i (= R_m l/2)$ in Fig. 7 is attributable to the different sample widths used. 2) For a given geometry, B_m narrows while the maximum value of R_m increases with increasing bias field (Fig 8).

At the higher frequencies considered, some of the theoretical approximations, i.e., $\alpha_0 l$, $\beta_0 l \ll 1$, and absence of ohmic loss, are not well satisfied. Furthermore, accurate impedance measurements become difficult. These factors account for the poorer theoretical–experimental agreement observed. The theory is expected to become less accurate as the width of the strip is decreased since the uniform current approximation becomes poorer and ohmic losses more significant.

Although the physical parameters considered to date are convenient for obtaining an accurate correlation between theory and experiment, in a practical device design a considerably broader excitation bandwidth than previously indicated is desirable. The wide bandwidth can be achieved by narrowing the microstrip width, as shown in Fig. 9. Note that for widths $b < 5d$, several hundred megahertz excitation bandwidths are possible.

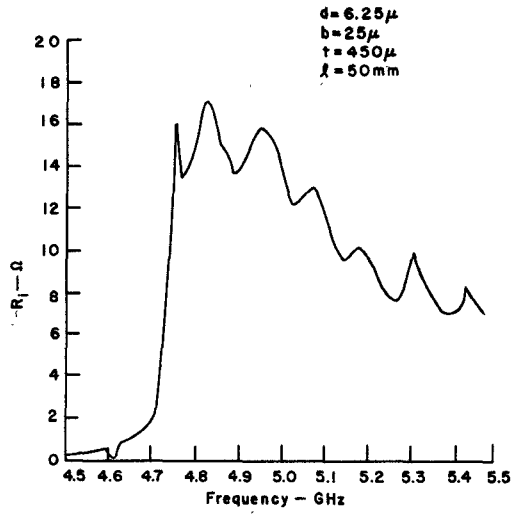

Fig. 10. Measured input impedance for configuration B [Fig. 1(b)].

Experimental results for configuration B are shown in Fig. 10. No meaningful comparison with theory is possible because of the experimental parameters used. The very narrow excitation strip gives rise to a high value of impedance for the YIG section, and no matching from the 50-Ω microstrip to the YIG section was employed. It is evident from Fig. 10 that substantial mismatch does occur. However, in general, it can be seen that the bandwidth of R_m can easily be several hundred megahertz wide.

VI. SUMMARY

The model developed for excitation of MSSW with microstrip circuitry has been shown to be in excellent agreement with experimental observations. The loss from the EM wave propagating along the microstrip to the MSSW system can be experessed in terms of an equivalent resistance R_m per unit length. When MSSW excitation is carried out by means of a shorted transmission line of length l, the equivalent MSSW radiation resistance can be expressed as $R_m l/2$ for a wide range of parameters of experimental interest. In contrast to conventional SAW excitation, essentially unidirectional transduction is possible. Finally, by making the microstrip approximately five times the film thickness or smaller, more than 500-MHz bandwidth is achievable. This is adequate for most projected MSSW applications [4], [10], since dispersion and not excitation then becomes the main bandwidth-limiting mechanism.

ACKNOWLEDGMENT

The authors wish to thank A. I. Braginski of the Westinghouse Research Laboratories for supplying the YIG samples and C. Banks for assistance in the measurements.

REFERENCES

[1] J. D. Adam, J. H. Collins, and J. M. Owens, *Electron. Lett.*, vol. 9, p. 557, 1973.
[2] J. B. Merry and J. C. Sethares, "Low loss magnetostatic surface waves at frequencies up to 15 GHz," *IEEE Trans. Magn. (1973 INTERMAG Conf.)*, vol. MAG-9, pp. 527–529, Sept. 1972.
[3] W. L. Bongianni, *J. Appl. Phys.*, vol. 43, p. 2541, 1972.
[4] A. K. Ganguly, C. Vittoria, and D. Webb, in *1974 AIP Conf. Proc. Magnetism and Magnetic Materials*, pp. 495–496.
[5] Y. S. Wu and F. J. Rosenbaum, *J. Appl. Phys.*, vol. 45, p. 2512, 1974.
[6] C. Vittoria and N. D. Wilsey, *J. Appl. Phys.*, vol. 45, p. 414, 1974.
[7] D. F. Vaslow, "Group delay time for the surface wave on a YIG film backed by a grounded dielectric slab," *Proc. IEEE (Lett.)*, vol. 61, pp. 142–143, Jan. 1973.
[8] T. J. Gerson and J. S. Nadan, "Surface electronic modes of a ferrite slab," *IEEE Trans. Microwave Theory Tech.*, vol. MTT-22, pp. 757–763, Aug. 1974.
[9] H. A. Wheeler, "Transmission-line properties of parallel strips separated by a dielectric sheet," *IEEE Trans. Microwave Theory Tech.*, vol. MTT-13, pp. 172–185, Mar. 1965.
[10] W. L. Bongianni, *Microwave J.*, vol. 17, p. 49, 1974.